



Winds and tides of Ligeia Mare, with application to the drift of the proposed time TiME (Titan Mare Explorer) capsule

Ralph D. Lorenz^{a,*}, Tetsuya Tokano^b, Claire E. Newman^c

^a JHU Applied Physics Laboratory, 11100 Johns Hopkins Road, Laurel, MD 20723, USA

^b Institut für Geophysik und Meteorologie, Universität zu Köln, Albertus-Magnus-Platz, 50923 Köln, Germany

^c Ashima Research, 600 S. Lake Avenue Suite 104, Pasadena, CA 91106, USA

ARTICLE INFO

Article history:

Received 11 October 2010

Received in revised form

11 December 2010

Accepted 22 December 2010

Available online 13 January 2011

Keywords:

Titan

Wind

Tide

Spacecraft mission

Global circulation mode

Ligeia Mare

ABSTRACT

We use two independent General Circulation Models (GCMs) to estimate surface winds at Titan's Ligeia Mare (78° N, 250° W), motivated by a proposed mission to land a floating capsule in this ~500 km hydrocarbon sea. The models agree on the overall magnitude (~0.5–1 m/s) and seasonal variation (strongest in summer) of windspeeds, but details of seasonal and diurnal variation of windspeed and direction differ somewhat, with the role of surface exchanges being more significant than that of gravitational tides in the atmosphere. We also investigate the tidal dynamics in the sea using a numerical ocean dynamics model: assuming a rigid lithosphere, the tidal amplitude is up to ~0.8 m. Tidal currents are overall proportional to the reciprocal of depth—with an assumed central depth of 300 m, the characteristic tidal currents are ~1 cm/s, with notable motions being a slosh between Ligeia's eastern and western lobes, and a clockwise flow pattern.

We find that a capsule will drift at approximately one tenth of the windspeed, unless measures are adopted to augment the drag areas above or below the waterline. Thus motion of a floating capsule is dominated by the wind, and is likely to be several km per Earth day, a rate that will be readily measured from Earth by radio navigation methods. In some instances, the wind vector rotates diurnally such that the drift trajectory is epicyclic.

© 2011 Elsevier Ltd. All rights reserved.

1. Introduction

The Titan Mare Explorer (TiME—Stofan et al., 2010) is a Discovery mission concept, recently proposed to NASA. The concept was initially developed in a NASA-funded Discovery and Scout Mission Capability Enhancement (DSMCE) study which sought to explore affordable mission concepts that would be enabled by an efficient long-lived power source, the Advanced Stirling Radioisotope Generator (ASRG), a unit that provides ~100 W of electrical power from ~500 W of heat evolved from plutonium decay. Such a unit allows long-lived operation at Titan, where both the thermal power and electrical power are required and solar power is impractical. The goals of the TiME mission are to measure the composition of the liquid in Ligeia and to observe atmospheric and oceanic phenomena at the air:sea interface (e.g. evaporation, generation of wind-driven waves) with cameras and a suite of meteorology and physical properties instrumentation, including a depth sounder.

The TiME mission features a launch in 2016, with direct entry from its interplanetary trajectory into Titan's atmosphere in July 2023. After parachute descent and splashdown into Ligeia Mare, it

would operate for a nominal duration chosen (not limited by power or geometry) to be 6 Titan days. The vehicle communicates direct to Earth and, in principle, it could be possible to maintain at least intermittent contact for several years after arrival: the Earth finally sinks below the horizon as seen from Ligeia in 2026.

It is of interest to consider how far and fast the vehicle may move on the surface of Ligeia, to determine if or when approach to a shoreline can be anticipated, to estimate the length of a likely sonar depth profile, and to assess what environmental factors can be estimated by measuring the drift. To that end, this paper summarizes model information on winds and tides. Although these model studies were motivated by the TiME mission, they will be of interest for studies of Titan oceanography in that winds may yield observable wave roughness as well as azimuthal variations in shoreline morphology. We begin, however, with a brief introduction to Ligeia observations by Cassini to date.

2. Observations and morphology

Ligeia Mare (Fig. 1) was first identified in the Cassini T25 Synthetic Aperture Radar (SAR) image acquired on February 27, 2007 and parts were re-observed on T28 and T29 six and eight weeks later: the corresponding Titan season, described by the

* Corresponding author. Tel.: +1 443 778 2903; fax: +1 443 778 8939.
E-mail address: Ralph.Lorenz@jhuapl.edu (R.D. Lorenz).

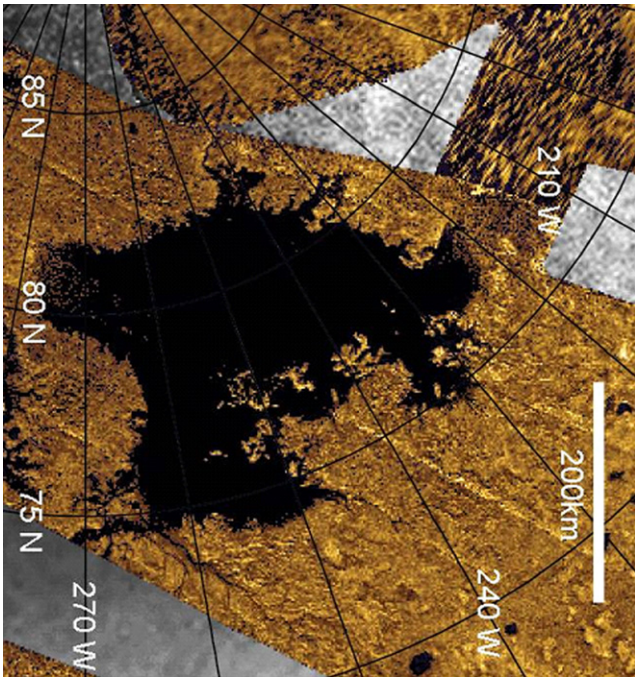


Fig. 1. Polar stereographic projection of a mosaic of Cassini SAR images (gold), showing the T-shaped Ligeia Mare.

Solar Longitude L_s , is $L_s=331^\circ$, about two thirds of the way between Northern Winter Solstice ($L_s=270^\circ$) and Northern Spring Equinox ($L_s=0^\circ$).

As with other Titan lakes (e.g. Stofan et al., 2007; Paillou et al., 2008), Ligeia is very dark in the SAR images, suggesting a very smooth surface. Radiometry data (Janssen et al., 2009) indicate a brightness temperature of 88.5 K, consistent (assuming a physical temperature of $\sim 90\text{--}92$ K) with a flat surface with a dielectric constant of 1.7 ± 0.1 , as would be expected with a liquid ethane/methane composition. Unlike the shallow margins of Ontario Lacus in the south, where an appreciable bottom echo can be detected (Hayes et al., 2010), almost all of Ligeia is pitch-black to the radar observations above (a striped appearance in raw images is due to the different noise floor in the images used to make the radar mosaic).

Morphologically, Ligeia seen with the 270° W meridian vertical (north up) is roughly T-shaped, with a West branch, an East branch and a South branch. Several large river channels appear to drain into Ligeia, most notably at the SouthWestern corner (75° N, 265° W) and at the northernmost point (80° N, 240° W). Overall the outline is of a ria coastline, indicative of a geologically recent rise in liquid level such that river valleys are drowned: the existence of many islands (particularly on the Southeastern side) is also consistent with this picture. A couple of somewhat straight edges on the Western side attest to possible tectonic influences on the outline. The geological history of Ligeia, therefore, appears complex and thus the mechanism by which the basin was formed in the first place is not obvious. The stippled appearance at the northwestern corner suggests (by analogy with Ontario Lacus) that this area may be shallow.

The largest radar-dark (and therefore likely deep) region is centered at about 80° N, 245° W: a 100 km circle centered on this point has $>99\%$ of radar pixels (averaged over 1 km areas) below -13 dB, and thus likely liquid-covered. Over 95% of the pixels thus defined are darker than -20 dB, and thus (by analogy with Ontario Lacus bathymetry) are greater than 6 m deep. A fuller analysis of all the available radar data (some areas of Ligeia have

been observed 2–3 times, at different incidence angles) will be the subject of future work.

Ligeia is also visible in the $2\ \mu\text{m}$ VIMS mosaic in Brown et al. (2008) although the resolution is too poor to learn anything new. Similarly, it can be identified in the 938 nm mosaic by Turtle et al. (2009). However, these early images under far-from-ideal conditions show promise for new findings as new and better observing opportunities arise in the Cassini Solstice mission as the subsolar latitude increases in the next few years. (In fact it is interesting to note that atmospheric scattering permitted the detection of Ligeia's outline in these optical observations even though it was close to, or even beyond, the geometric terminator.)

As Titan's second-largest sea, Ligeia is a significant contributor to Titan's organic inventory (Lorenz et al., 2008). The composition of Ligeia Mare is not known, although it is presumably dominated by ethane and methane. A near-infrared spectroscopic signature of ethane was detected in Ontario Lacus (Brown et al., 2008) although it is not clear if that constituent is dominant there, nor whether the composition of northern seas should be the same as Ontario, since seasonal or Croll–Milankovich astronomical forcing (Aharonson et al., 2009) may favor a more volatile composition in the north in the present epoch. The composition of Titan seas in thermodynamic equilibrium with the atmosphere (assuming the 5% methane mixing ratio in the equatorial atmosphere applies at the poles) is 76–79% ethane (Cordier et al., 2009). However, some disequilibrium is possible due to thermal inertia effects (e.g. Tokano, 2009a, 2009b) and methane evaporation from the sea surface (e.g. Mitri et al., 2007), so the composition may be more or less ethane-rich.

3. Winds

We simulate the winds on Ligeia with a three-dimensional atmospheric GCM that is coupled to a one-dimensional sea energy balance (thermal stratification) model, as described in Tokano (2009a) and hereafter referred to as the 'Köln (Cologne) model'. The atmospheric model solves a set of primitive equations (with hydrostatic approximation) on gridpoints to predict the temporal evolution of the wind, surface pressure, temperature and methane mixing ratio. The model domain consists of 32 longitudinal, 24 latitudinal and 60 vertical gridpoints. Gaseous methane is treated as a passive tracer, and is subject to global transport as well as condensation, precipitation and evaporation. Clouds and precipitation (hydrometeors) are not treated as separate prognostic quantities, but are diagnosed from the change in the methane relative humidity. Only large-scale condensation (stratiform condensation) is taken into account, i.e. subgrid-scale moist convection is not treated. The 3-dimensionality of the model enables modeling of breeze induced by temperature contrasts between the sea area and the surroundings. The prescribed seas are assumed to have a lower albedo and higher thermal inertia than the surrounding dry land. (The sea is assumed to have an albedo half as large as land. The thermal inertia of the sea is dependent on the composition and instantaneous temperature, but is 2–3 times larger than that assumed for land. The sea energy balance model predicts the sea surface temperature considering absorption of sunlight, emission of thermal infrared radiation, sensible heat flux between sea and air, latent heat of evaporation and convective mixing.

As discussed in Tokano (2009a), there is a significant effect of the assumed sea composition on the predicted meteorology. Specifically, if the sea is methane-rich, methane evaporation absorbs much of the incident solar energy and leads to gentler large-scale winds than for an ethane-rich composition where the sunlight is converted more into sensible heat. In this paper, we

principally report results for the ethane-rich case (78% C₂H₆, 17% CH₄, 5% N₂ by volume) as these are more conservative (in the sense of leading to higher winds). In the Köln model, Ligeia occupies three grid cells.

To at least partly evaluate the robustness of the model predictions, we also examine the output of an entirely independent model, TitanWRF (the Titan implementation of PlanetWRF, the Planetary Weather, Research and Forecasting model, Richardson et al., 2007). Like the Köln model, TitanWRF solves a set of primitive equations (with hydrostatic approximation) on grid-points to predict the temporal evolution of the wind, surface pressure and temperature, but runs at slightly higher resolution in the horizontal (with 64 longitudinal and 36 latitudinal gridpoints) and has 54 vertical gridpoints up to ~400 km above the surface.

Though TitanWRF is a three-dimensional model (Newman et al., 2008) and includes the effect of diurnally varying heating and gravitational tides, the version used here assumes a featureless, solid surface (i.e. the albedo and thermal inertia, etc. of the surface is uniform everywhere, with no separate values for sea surface properties). TitanWRF originally produced only weak stratospheric superrotation, as shown in Richardson et al. (2007), but the latest version of the model (described in Newman et al., 2010) now produces strong stratospheric superrotation very similar to that observed by CIRS (e.g., Achterberg et al., 2008). TitanWRF thus has significantly stronger upper level winds than produced in the Köln model, but its lower tropospheric windspeeds are similar to those measured by the Huygens probe (Newman et al., 2010) and both models produce winds of similar magnitude close to the surface.

A general problem of Titan GCMs is the scarcity of tropospheric data against which the models could be validated. Nevertheless, both GCMs roughly reproduce the latitudinal surface temperature gradient retrieved by Cassini's thermal spectra (Jennings et al., 2009). Considering the strong control of the surface temperature on the tropospheric circulation pattern this agreement is one important piece of evidence that the models are capturing principal elements of the circulation. Subtle differences in the parameterizations of the surface–atmosphere exchange processes, which would affect the wind prediction, certainly exist. However, most differences seem to result from the inclusion or omission of seas or the different assumptions about sea compositions in the model.

It is of interest that the Köln model (Fig. 2) predicts the summer onset of strong (> 0.5 m/s) wind around $L_s \sim 45^\circ$, (calendar year 2013), rather later than the $L_s \sim 15^\circ$ onset for Kraken,

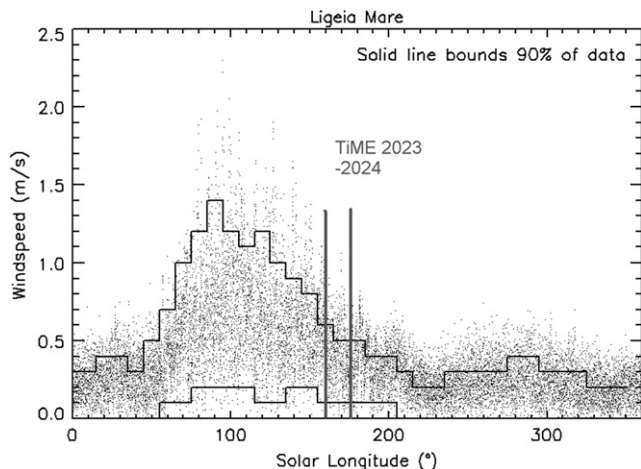


Fig. 2. Near-surface winds as a function of season predicted by the Köln model for a C₂H₆-rich sea composition. The TiME mission epoch is after the summer freshening of winds at Ligeia.

further south (not shown). The TitanWRF model, in contrast, suggests that winds at Kraken should have increased shortly before equinox $L_s=0^\circ$ (e.g. Figure 5 of Lorenz et al., 2010). While the reason for this difference is not immediately obvious, a possible explanation for this disparity is the different surface temperature evolution in these two models. Surface wind refreshes with increasing horizontal surface pressure contrast, which is strongly affected by the surface temperature. In the Köln model, the increase of the sea surface temperature begins later in spring because of the large assumed thermal inertia. The delay of the warming is even more pronounced in Ligeia, which is located at higher latitudes than the major part of Kraken Mare.

It was recognized before Cassini's arrival that roughening of the sea surface by wind-driven waves might be detectable in sunglint observations (e.g. Lorenz et al., 2003) although geometrically (since the extensive seas are found near the north pole) it is only now that opportunities for such measurements are coming about. A specular reflection (sunglint) was observed by VIMS in summer of 2009 (Stephan et al., 2010) and suggests that the region observed (Jingpo Lacus, a lake nearby and perhaps connected to Kraken Mare) was very smooth—a recent quantitative analysis (Barnes et al., 2011) suggests the roughness was characterized by a less than 0.1° root mean squared surface slope variation. Radar backscatter is another diagnostic of roughness. A radar observation of Ligeia Mare in T64 (December 2009) does not appear to indicate any appreciable brightening of the surface, implying that winds are still below the wave generation threshold (whatever that may be—it is composition-dependent, but likely in the range 0.5–1 m/s (Lorenz et al., 2005, 2010)). Thus, unfortunately observations so far give little information on what surface windspeeds are or will be.

Since it is impossible to design spacecraft or instruments to function at infinite windspeeds, it is useful for engineering purposes to examine the wind probability density distribution, to determine design values that will be exceeded at some acceptable probability or frequency, or equivalently to report the frequency with which a given windspeed is exceeded. Given the lack of observations, we must, therefore, examine the statistics of the model winds.

For the TiME season $L_s=150^\circ-170^\circ$, it is seen (Fig. 3) that the Köln model windspeeds are much more narrowly distributed than over the year as a whole (Fig. 4). Winds of greater than 1 m/s are encountered less than 5% of the time. Note that many engineering analyses such as Monte Carlo studies report their results as if they had a Gaussian distribution—in this case, a 5% exceedance rate

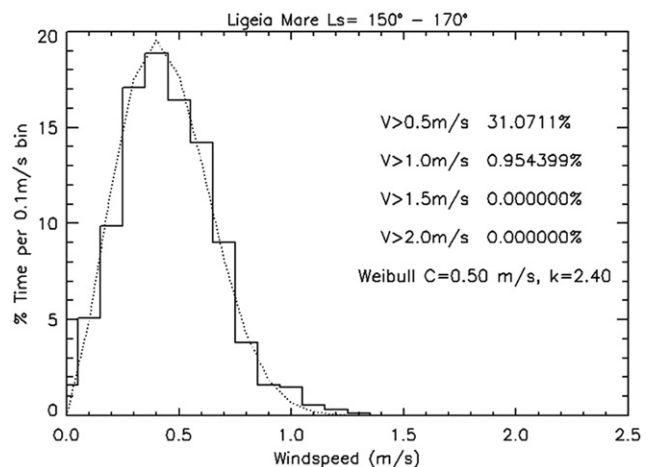


Fig. 3. Köln model (C₂H₆-rich) windspeed predictions for the TiME epoch (late summer). The windspeeds have a near-Gaussian distribution, and rarely exceed 1 m/s.

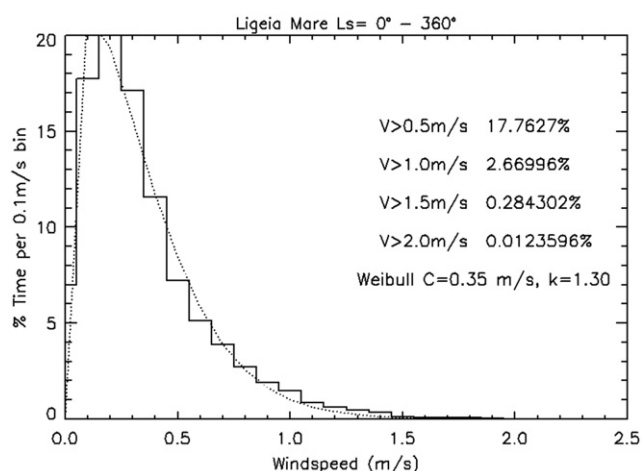


Fig. 4. Surface windspeeds at Ligeia in the Köln model (C_2H_6 -rich) for the whole Titan year. These annual Titan winds (sampled 24 times per Titan day) have a somewhat exponential distribution—the very rare winds above 1.5 m/s occur in the peak of summer.

would be considered a ‘2-sigma’ wind limit. However, windspeeds tend not to have a Gaussian distribution, but are skewed (not least because a negative windspeed is unphysical) and a Weibull or similar distribution is often used. Weibull statistics are widely used in the ocean engineering and wind energy communities, and have been used to succinctly describe the statistics of Mars surface winds measured by the Viking landers (Lorenz, 1996). The Weibull distribution has a cumulative probability $P(>U)$ exceeding the windspeed U given by the expression $P(>U) = \exp(-[U/C]^k)$ where C is a scale speed and k is a shape parameter: the shape parameter allows the function to describe both near-symmetric distributions (similar to Gaussian) as well as highly skewed ones such as the exponential. The Weibull parameters that fit the Köln model winds are provided in Figs. 3 and 4.

In summary, the models are comparable (Fig. 5) in their prediction of surface windspeeds: the most conservative case appears to be the C_2H_6 -rich Köln model, with most probable windspeeds of ~ 0.5 m/s; winds are rarely ($< 5\%$) above 1 m/s during the TiME epoch and do not exceed 1.5 m/s during that season. The Köln model with a CH_4 -rich sea has the smallest winds (almost always < 0.5 m/s). Note that these results refer to large-scale circulation—it is possible that a CH_4 -rich sea may be associated with stronger local methane weather (i.e. more frequent rainstorms) that may cause brief gusts on small scales that are larger than indicated here. A meso-scale model could simulate such small features better, but on the other hand the seasonal variation of the surface wind is also strongly affected by the global surface pressure distribution, which can only be faithfully predicted by a global model. Thus, a nested combination of global and meso-scale models would likely yield the best estimates of winds.

The wind directions predicted by the models (Fig. 6) vary over the course of a Titan day, and differ between the models. The C_2H_6 -rich Köln model indicates predominantly retrograde winds, whereas the other models suggest prograde. Significantly, the near-surface meridional winds in all models are found blowing both north and south, and with comparable magnitude to the east–west component.

4. Tides

Tides in a global sea of liquid hydrocarbons were considered analytically by Sagan and Dermott (1982) and Sohl et al. (1995).

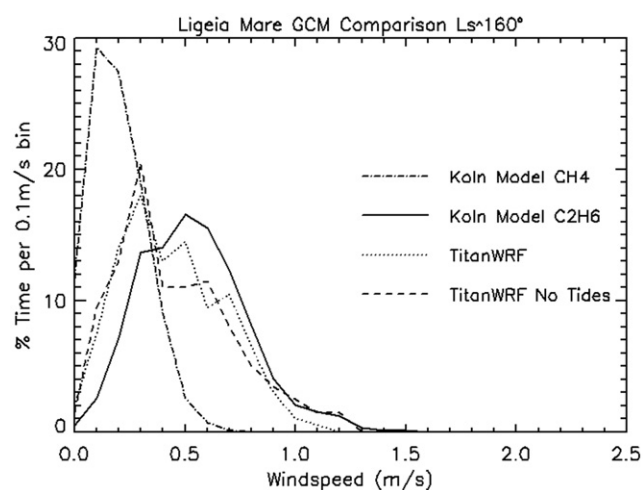


Fig. 5. Model intercomparison for the TiME season. The Köln- CH_4 , TitanWRF and Köln- C_2H_6 models have most probable windspeeds of ~ 0.1 m/s, 0.3 m/s and 0.5 m/s, respectively. There is minimal difference between the TitanWRF cases with and without gravitational tides. In no model do winds exceed 1.3 m/s for more than 0.5% of the time.

Tides in more restricted bodies of liquid were considered by Lorenz (1994) and Dermott and Sagan (1995). Tides were modeled in some detail with a numerical model by Sears (1995), which also examined some idealized cases of nonglobal oceans. These studies noted the stationary (~ 100 m) tidal bulge, and that this grew and shrank by $\sim 9\%$ over a Titan orbit.

More recently, following Cassini’s findings, Tokano (2010) adapted a terrestrial numerical tidal model to Titan seas (specifically Kraken Mare and Ontario Lacus) with notional bathymetry. The model is designed as a 3-dimensional baroclinic ocean circulation model with tidal forcing. In this way, the model can be optionally used to simulate the thermal circulation and wind-driven circulation in addition to tides. However, in this study we turn off the solar heating and wind forcing as baseline model, so the model is run as a barotropic tidal model. It was previously shown for Kraken Mare that solar heating of the sea surface in summer may generate internal tides in the presence of a strong thermal stratification (Tokano, 2010). In this case, the flow pattern in deeper parts of the sea can be opposite to that near the sea surface. However, the surface flow pattern is barely affected by this, so we do not expect an impact on a capsule floating on the sea surface. Strong wind would deflect the surface tidal flow toward the surface wind direction, but flow speed of the top layer of Ligeia is likely to be less sensitive to the windspeed than to the depth of the sea, except perhaps during extreme gusts. The model equations are analogous to those of an atmospheric GCM, but the major difference is the Boussinesq approximation according to which density variations are neglected in the equations except in terms that are multiplied by the gravitational acceleration. This approximation is considered valid in Titan’s shallow seas, in contrast to the hypothetical deep subsurface water ocean.

Here, we apply the same model to Ligeia. The outline of Ligeia was digitized from map-projected radar images, and a notional bathymetry was assumed (Fig. 7).

Tidal accelerations due to Saturn (Fig. 8) are calculated analytically, and in effect lead to a changing tilt in the local vertical. Because the tidal forcing period on Titan is long compared with the propagation time of shallow-water waves, the tide is essentially an equilibrium one, without resonant effects (e.g. Lorenz, 1994) and the tidal amplitude (Figs. 9 and 10) is

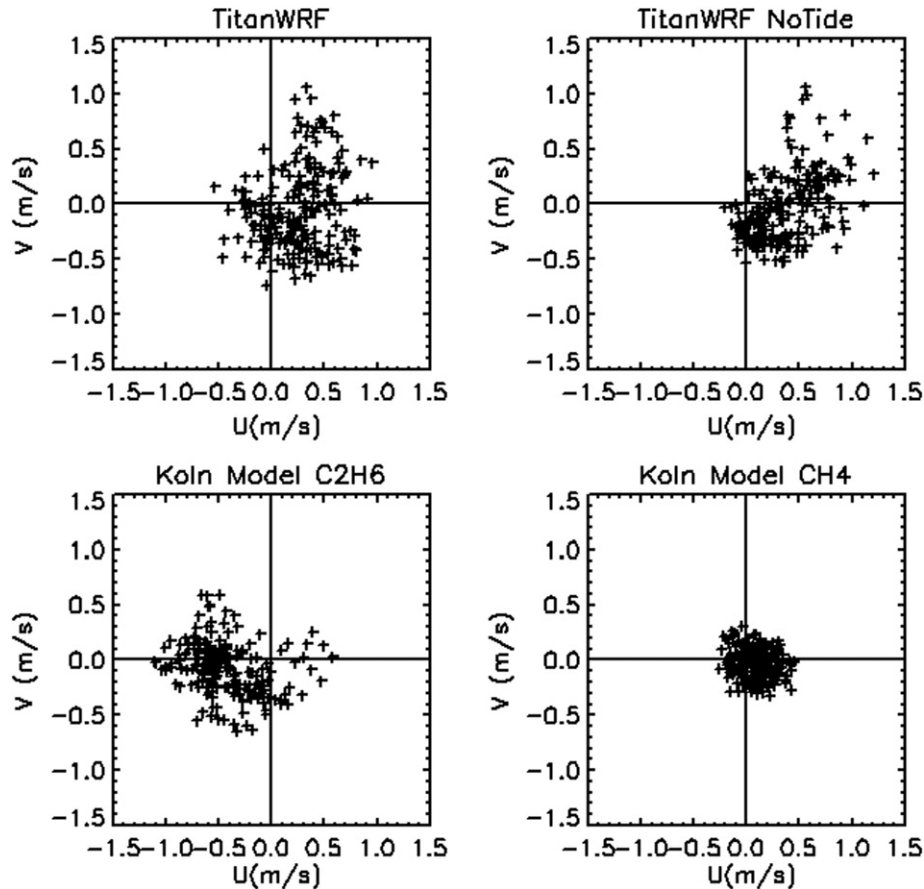


Fig. 6. Model intercomparison—instantaneous winds over a period around $L_5 \sim 156$ are plotted as crosses. The TitanWRF model shows generally prograde (westerly) winds in both tide and no-tide cases, while the Köln model has weak prograde winds for a CH_4 -rich sea composition, while the C_2H_6 -rich composition has retrograde (easterly) winds. In all cases, the north–south component of wind can be comparable with the zonal component.

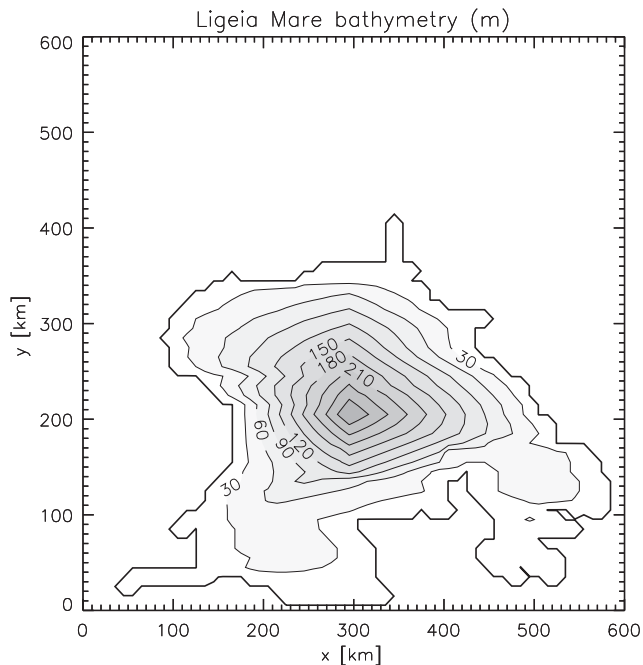


Fig. 7. An assumed (not measured) idealized bathymetry for Ligeia Mare, derived assuming a central depth of 300 m.

independent of the assumed bathymetry. This analysis assumes that Titan itself is a rigid sphere and does not itself deform during a tidal cycle: introduction of body tides would be an interesting future exercise in that any lag in the response of the ‘solid’ body (noting that Titan may have a partly liquid interior) may result in a change in the direction of the effective acceleration on the surface liquids from that modeled here. However, the magnitude of the effective acceleration will be generally less than that modeled here. It can be seen (Fig. 9) that the basic tidal cycle is one of liquid sloshing from the eastern lobe to the western and vice-versa.

The tidal amplitudes (see also Fig. 10) are independent of depth (for realistic values of depth—recall that the radar-darkness suggests depths over most of Ligeia of > 6 m, far too deep for resonant tides to occur). However, the tidal currents do vary with depth—in effect a triangular wedge of liquid ~ 0.5 m high and ~ 200 km wide must cross the central meridian of Ligeia twice each Titan day. This defines a characteristic volume flow rate ($\sim 0.1 \text{ km}^3$ per meter of the meridian) and thus the corresponding flow speed will depend on the liquid depth. 0.1 km^3 per ~ 8 days corresponds to $\sim 0.1 \text{ m}^3/\text{s}$ per meter of meridian: if the liquid depth is ~ 100 m (i.e. the sea is a channel with a cross-sectional area of $100 \text{ m}^2/\text{m}$ of meridian) then the corresponding flow speed is $\sim 0.1 \text{ cm/s}$. Clearly the details vary (in interesting ways) but this order-of-magnitude calculation helps to set the context for the numerical model results.

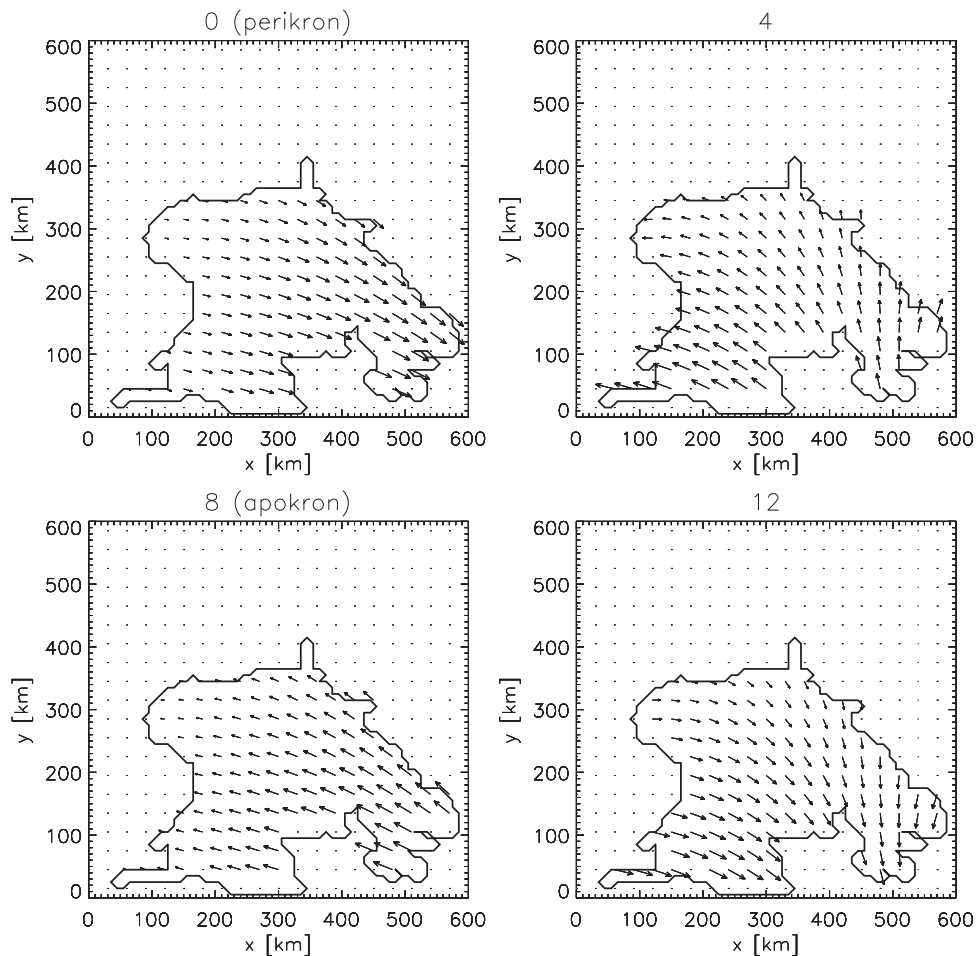


Fig. 8. Direction of the tidal acceleration on Ligeia, assuming a rigid, spherical Titan as a function of orbital phase (numeral above the plot refers to the earth day relative to periapsis). The lengths of the arrows scale with the magnitude of the acceleration.

Should Ligeia Mare be somehow connected with adjacent lakes by channels, a focused tidal flow similar to that predicted for a strait in the southern portion of Kraken Mare (Tokano, 2010) might exist in such channels. However, as this is speculative at this stage, we refrain from pursuing this issue in the present study.

Given the assumed bathymetry, the maximum tidal currents (Fig. 11) of ~ 1 cm/s are encountered in the eastern lobe. However, this depends explicitly on the assumed depth—if this lobe were deeper, the currents would be correspondingly weaker. The fluid dynamics are such that the sloshing flow does include a rotational component, and a large clockwise flow pattern (we avoid referring to it as a ‘gyre’ since in terrestrial oceanography this usually implies a role of the Coriolis effect, which is in fact not the case here) is seen in the central, deepest part of Ligeia (Fig. 12).

As we shall now discuss, the effect of these tidal currents on the motion of a floating capsule is likely to be small compared with the effects of the wind. However, it is of interest that these tidal motions should assure substantial mixing of Ligeia’s waters and thus make the composition somewhat uniform (the time t or a parcel of liquid to be advected across Ligeia is ~ 1 Earth year, rather less than the duration of a season).

Additionally, the turbulent flow associated with tidal currents of 1 cm/s is likely to be able to keep solid particulates suspended in the liquid: Lunine (1992) noted that the settling velocity of small particles of organics or ices would be quite small and might permit their suspension. Applying Stokes’ Law and representative

fluid properties, it is easily seen that sand-sized ice particles (0.1 mm radius) would have settling velocities in liquid ethane of only 1 mm/s. Convective mixing in cold seasons may also give rise to currents enough to cause suspension of solid particulates (Tokano, 2010b), as might solar heating in the uppermost layers.

It is possible that wind-driven currents in the liquid may be comparable with (or even exceed) these tidal currents, but the lack of convergence of the wind models and the dependence of both current types on liquid depth poses a challenge to quantitative predictions. However, the fact that tidal currents and convection alone can cause mixing and suspension is important to note.

5. Drift trajectories

The drift of floating objects at sea is a function of the motion of the liquid and of the air, with the relative contributions of the forces from these two fluids being a function of the cross-sectional areas above and below the ‘waterline’. The drift trajectories of objects can be used as a diagnostic of ocean currents if they barely float (e.g. athletic shoes released from a shipping accident, as described in the popular account ‘Flotsametrics’, Ebbemeyer (2009)), and so-called ‘drifting buoys’ are equipped with drogue parachutes suspended below the waterline to maximize the effect of ocean currents (and thus minimize the relative contribution of wind, e.g. Kirwan et al., 1975). On the other hand,

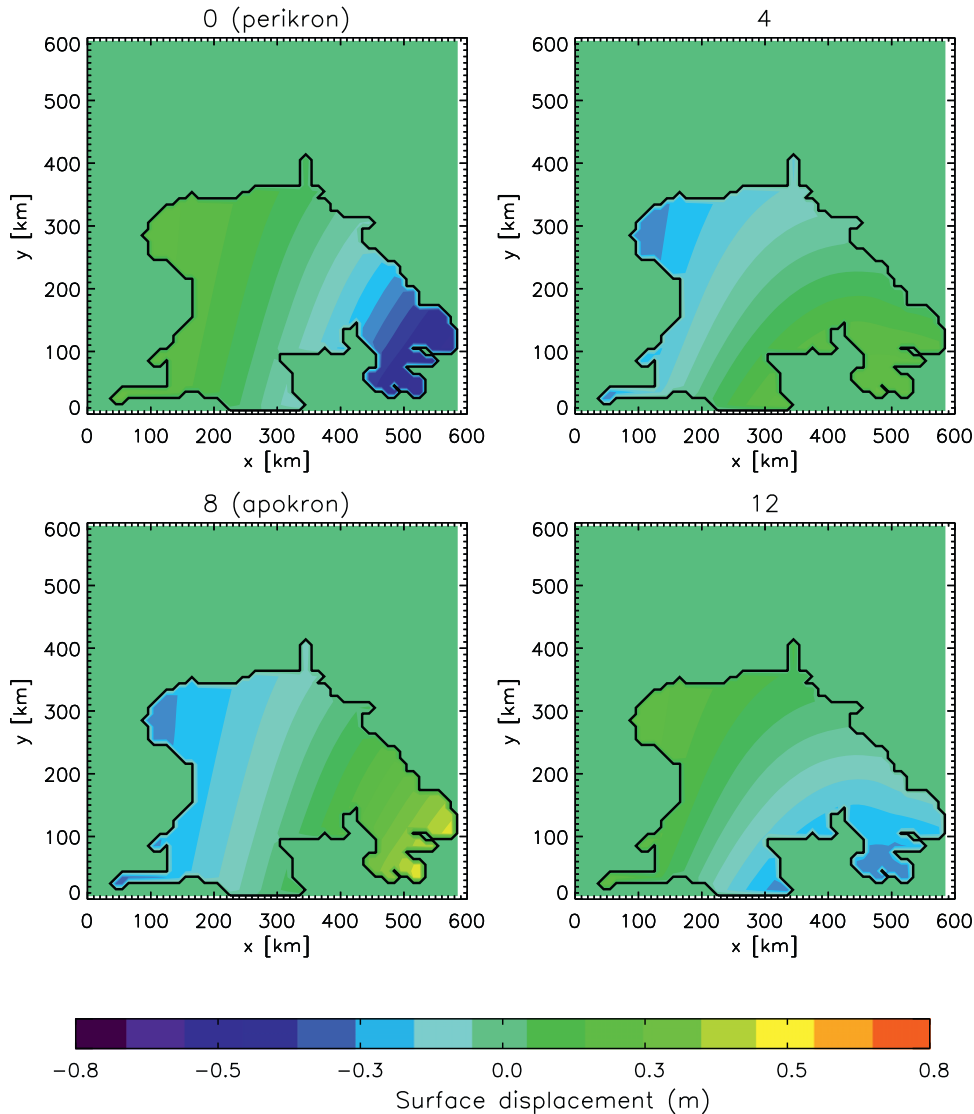


Fig. 9. Tidal heights for Ligeia Mare as a function of time. The peak amplitudes are at the Eastern and Western lobes. It is seen that the principal tidal effect is a slush from the western to eastern lobes of Ligeia.

of course, through much of history, military and commercial marine transport has been accomplished by shifting this balance in the other direction, by erecting large structures above buoyant vehicles—i.e. sails.

If we consider the vehicle fixed in the reference frame of the liquid, then we can equate the wind drag on the top of the capsule (atmospheric density ρ_a , windspeed U and drag area A_a) with that caused by the motion of the capsule moving at speed V through the liquid density ρ_w , with immersed drag area A_w . Thus, $\rho_a A_a U^2 = \rho_w A_w V^2$. (We refer to the force as drag—yet in the case of a sail, a substantial force orthogonal to the wind direction, thus ‘lift’, can be generated. We ignore this distinction in the present discussion: similarly, we refer to the lumped parameter ‘drag area’ to mean the product of the geometric area above and below the waterline with their respective drag coefficients).

The density of the TiME capsule (and, indeed this was the case for the Huygens probe – Lorenz 1992 – spacecraft fabrication methods are such that bulk densities of the order of $\sim 250 \text{ kg/m}^3$, half the density of liquid hydrocarbons, are typical) is such that the cross-section areas above and below (A_a and A_w) the waterline are approximately equal, and ignore any difference in drag coefficients. It, therefore, follows that the ratio of the drift speed

to the windspeed is the square root of the air: sea density contrast, i.e. $(V/U) \sim (\rho_a/\rho_w)^{0.5}$. For Titan this contrast is ~ 100 (compared with ~ 1000 on Earth) and thus the succinct result is obtained that the drift is one tenth of the windspeed: more careful evaluation of drag areas by models or wind tunnel tests might adjust this result by tens of per cent.

Thus, we can calculate the likely drift of the TiME capsule in Ligeia by changing its position at $\frac{1}{10}$ of the model windspeed. Note that this approach neglects any possible wind-driven currents, although these should be somewhat small if Ligeia is more than a few meters deep.

Fig. 13 shows an example trajectory using Köln model winds (the C_2H_6 -rich case winds are shown, since these are stronger and thus more interesting). It is seen that because the wind direction rotates throughout a Titan day that a somewhat epicyclic drift path is followed: this might be of interest in that since the track crosses itself, some intercomparison of measurements might be possible (e.g. measure temporal change at a given location, or measure seabed slopes in two directions at the crossover point). It is seen also that the overall drift is West-South-Westwards (WSW), although as discussed in Section 3, the net drift direction and distance would be different for other models.

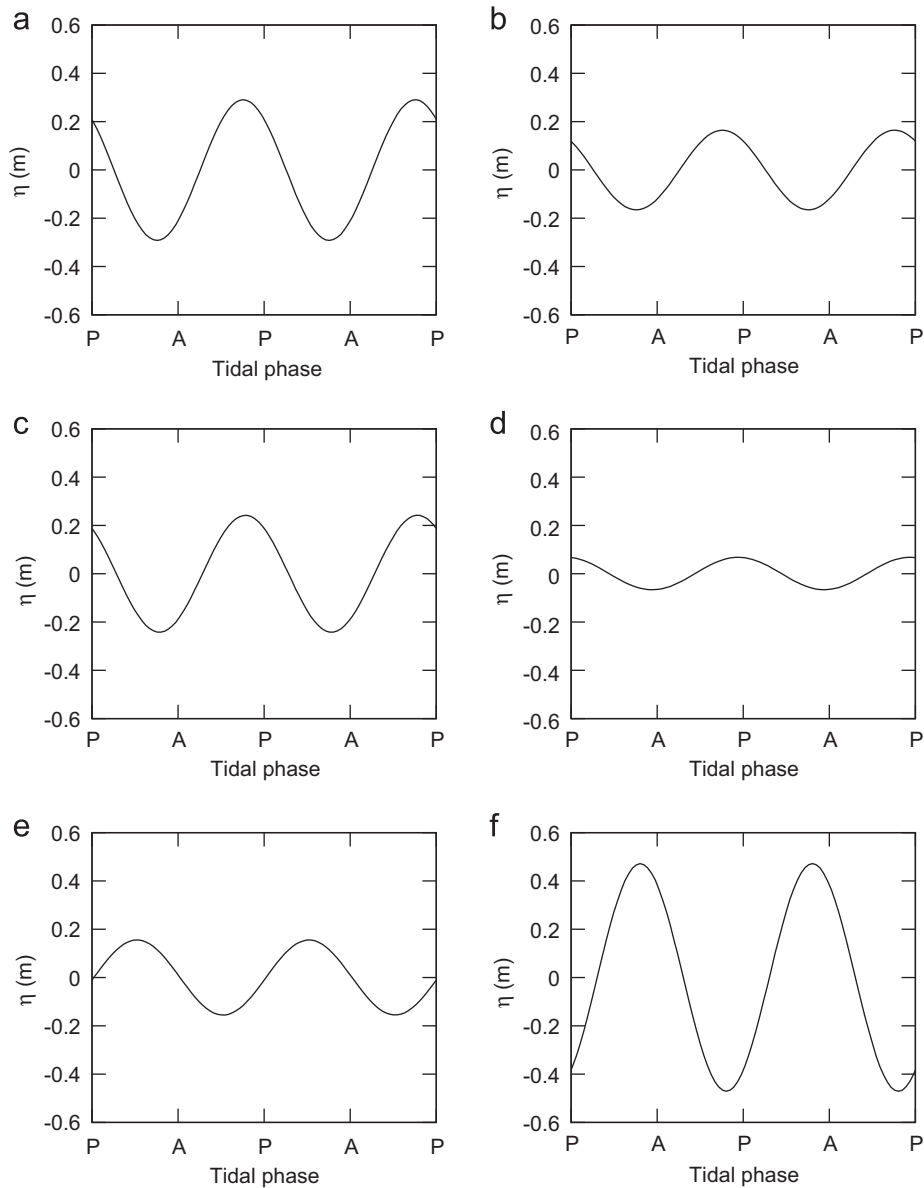


Fig. 10. Times series of tidal amplitudes at various locations in Ligeia for two consecutive Titan days. P and A denote the apoapsis and periapsis, respectively. Locations are (a) 82°N 80°W, (b) 82°N 70°W, (c) 78°N 80°W, (d) 79°N 70°W, (e) 75.5°N 70°W, (f) 77°N 50°W.

Fig. 14 shows the dispersion that may be expected (the Köln- C_2H_6 model is used throughout, but a suite of release times 1 Titan day apart are used). Fig. 15 shows the same trajectories, but as distance from release point as a function of time. It is seen that a drift of 150 km in 5 Titan days is typical, although the drift could be double this value.

In the CH_4 -rich case, the summer breeze is predicted to be weaker, so the drift would contain a smaller translation compared to rotary motions. While there is agreement between the Köln model and TitanWRF in the general seasonal pattern of the surface Hadley cell, the breeze represents a more uncertain wind system since it is largely controlled by the sea surface temperature. The sea surface temperature is affected by evaporation, convection and possibly also precipitation, which may have a different temperature than the sea.

Given such uncertainties in the wind predictions, Figs. 14 and 15 should not be regarded as exact predictions of the trajectories. Instead it exemplifies the possible range or shape of the drift trajectories.

6. Navigation

A natural question given the predicted motion is how well this motion can be determined: since we have shown that the motion will be dominated by wind, tracking the drift of the TiME probe can serve as an integral measure of the wind. Position information is important in setting observations (e.g. of depth) in context, and knowledge of the vehicle position may also be of interest if the vehicle is equipped with a propulsive or drag modulation capability, or indeed with an anchor. Even if the vehicle's motion cannot be controlled, it may be desirable to change observation sequences to optimize scientific return (e.g. to image a shoreline). Thus, in this section we consider how the position history may be reconstructed.

6.1. Doppler

Measurement of Doppler shift is a straightforward technique, used routinely on orbiters and probes. The measurement may be

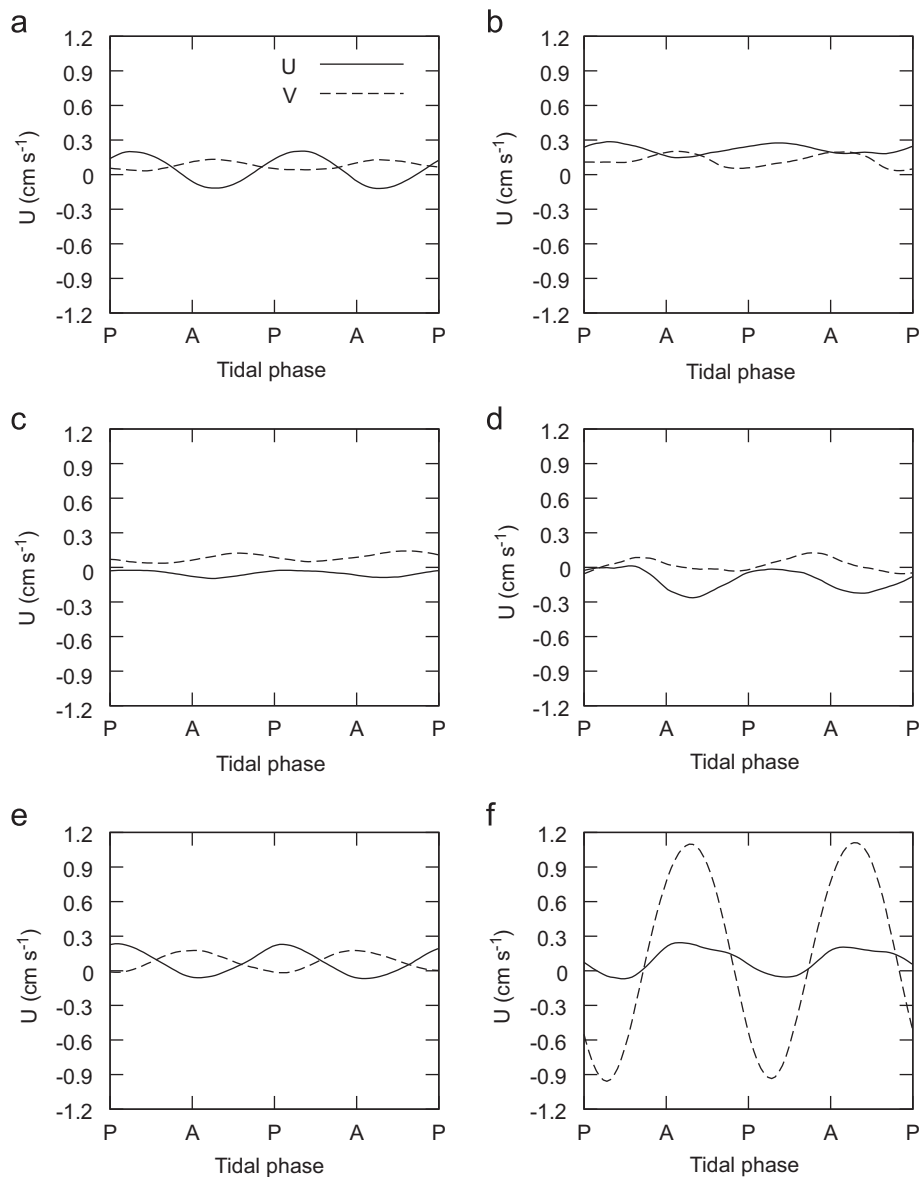


Fig. 11. Time series of tidal currents (solid line=zonal component U , positive eastwards; dashed line is meridional component V , positive northwards) at various locations for two consecutive Titan days. Locations are (a) 82°N 80°W, (b) 82°N 70°W, (c) 78°N 80°W, (d) 79°N 70°W, (e) 75.5°N 70°W, (f) 77°N 50°W.

implemented by coherent two-way communication, or by using a precision frequency reference on the probe (an Ultra-Stable Oscillator or USO). The navigation discussion hereafter is agnostic as to how the measurement is actually implemented.

The precision with which the range-rate (i.e. the projection of the vehicle's velocity onto the line of sight to the receiver on Earth) can be measured relates directly to the frequency precision $\Delta f/f$. In other words, the speed uncertainty $dV \sim c\Delta f/f$ where c is the speed of light.

If we assume the vehicle to be stationary with respect to Titan's surface, Titan's rotation induces a sinusoidally varying (once per Titan day) range-rate whose amplitude is directly proportional to the cosine of latitude: near the pole, this in fact makes Doppler quite a sensitive measure of position.

The Huygens USO, with a specified absolute $\Delta f/f$ (30 min) of 2×10^{-10} yielded a relative point-to-point variance in the 2.048 GHz S-band frequency measured on the ground of 0.1 Hz (i.e. $\Delta f/f$ of 4×10^{-12}), corresponding to a range rate of 0.11 mm/s. At Ligeia Mare, the range rate due to Titan's rotation will be of the order of 1 m/s, declining to zero when the probe and the Earth

have the same longitude. Thus, if the absolute transmit frequency were known to a precision comparable with the relative precision of the Huygens data, then the maximum range rate could be determined to about 1 part in 10^4 , and thus the latitude could in theory be determined (by measuring at intervals spread over 16 days) to about 0.1 km, or about 4 thousandths of a degree. In reality, there will be some uncertainty in the longitude, which maps into an uncertainty in the latitude implied by a given Doppler shift. Thus, the position determination is a somewhat iterative problem. However, while instantaneous Doppler measurement can be acquired in only a few seconds, most likely such data will be available for ~ 8 h communications sessions, during which Titan will rotate by $\sim 7^\circ$, producing a readily detectable change in Doppler shift over this period. Thus, although the position uncertainty is reduced considerably by measurements spanning several Earth days, even a single communications session may yield a useful 2-dimensional location estimate.

That said, in reality, we cannot assume the lander to be static. We may expect some (by definition unknown) drift velocity, of the order of 0.1 m/s, in which case the latitude can only be

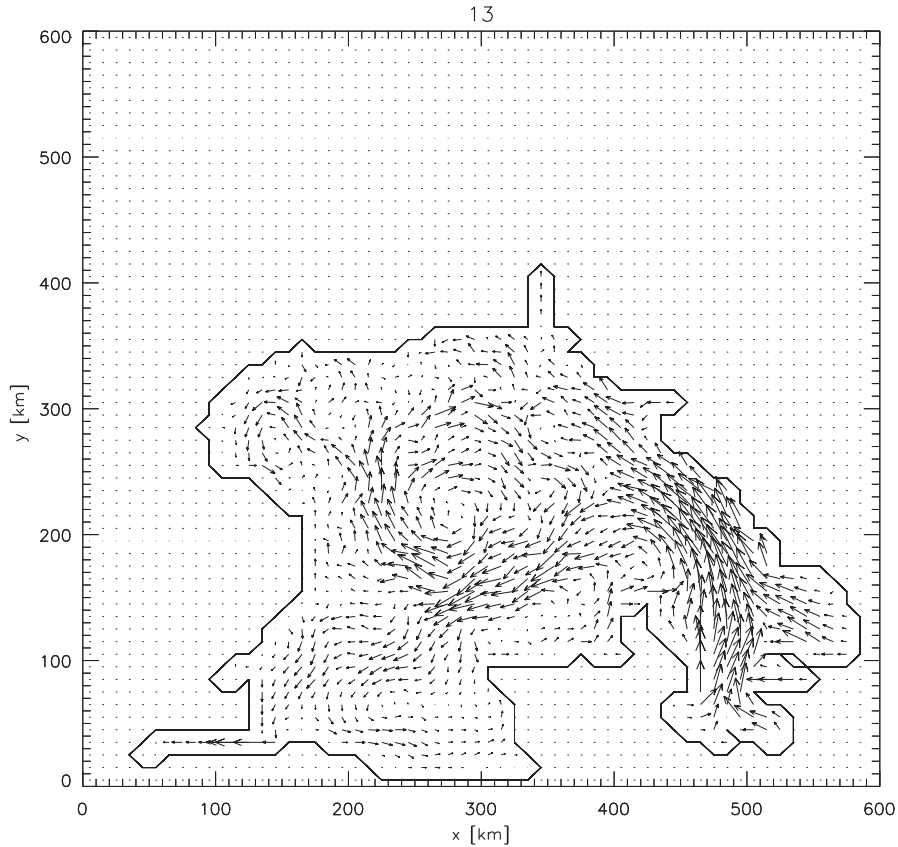


Fig. 12. Flow vectors 13 days after periapsis: note the relatively strong flow out of the eastern lobe, and the clockwise flow pattern in the center. Unit vector length is 1 cm/s.

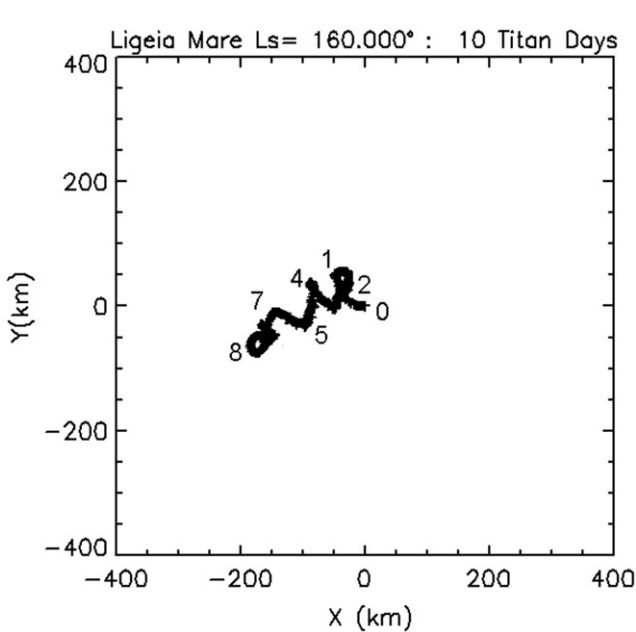


Fig. 13. Capsule drift at $(\frac{1}{10})$ the windspeed for the TiME season in the C_2H_6 -Köln model. The rotating wind vector leads to an epicyclic drift trajectory. Numbers on the curve indicate the Titan day after release.

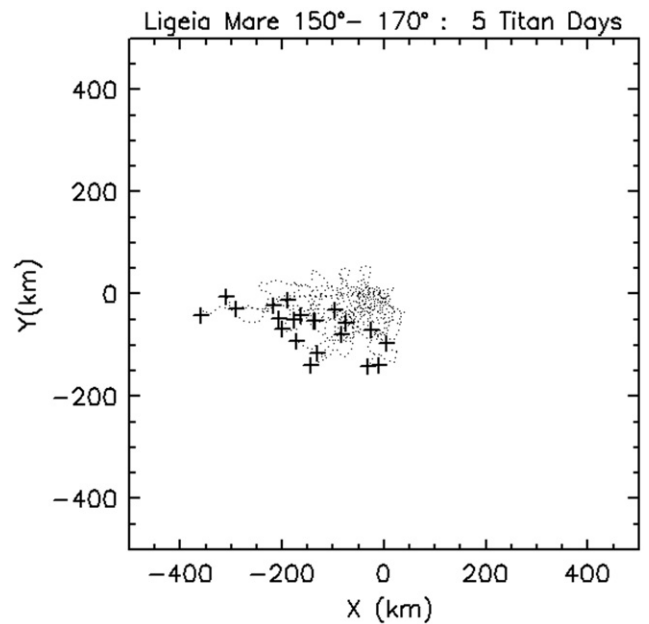


Fig. 14. Trajectories (dots) and end points after 5 Titan days each (crosses) for 18 release times (one Titan day apart) over the interval from $L_s=150^\circ$ to 170° in the C_2H_6 -Köln model. The differences are due to stochastic forcings (e.g. planetary waves) in the model, together with some seasonal change, but give an idea of the variation that may be expected.)

determined to about 100 km. Of course, if the position is known (e.g. from the delivery navigation), then the range-rate component of the drift velocity can be measured quite well. Again, while

individual instantaneous measurements will be ambiguous, a comprehensive analysis of data over 1 or more Titan days will yield a robust and accurate trajectory.

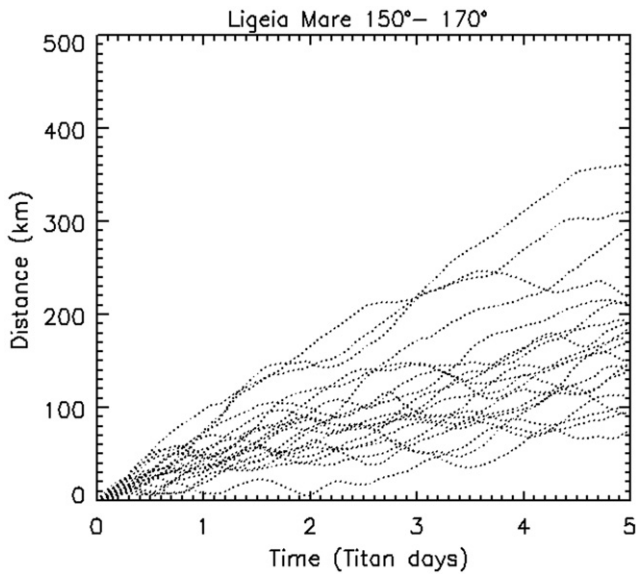


Fig. 15. Evolution of distance from start point of the drift trajectories as shown in Fig. 14.

6.2. Sun height measurement

The height of the sun above the horizon is a measure of how far the probe is from the subsolar point. Historically, this has been performed for centuries in terrestrial marine navigation by using a sextant. The maximum altitude of the sun is reached at local noon, and gives a direct measure of latitude if the date and solar ephemeris is known. Some longitudinal information can be obtained if a suitably accurate clock is available. Note that on Earth even today light intensity measurements via datalogging light meters are sometimes used to determine position of migrating animals in cases where GPS receivers are too heavy (e.g. birds) or otherwise unusable (e.g. marine mammals such as seals, e.g. Hill 1994).

Experiments with Mars sky imaging (M. Lemmon, personal communication) suggests that the solar position can be estimated to about 1° even when the sun is itself not in the image, providing a large part of the sky can be imaged so that isophote curvature can be measured. An all-sky imager can likely provide this capability, although it should be noted that this implies a measurement in the lander coordinate frame, not the Titan frame. A surface science imager, with higher spatial resolution, can likely measure the sun position, again in the lander frame, to about 0.2° , since the position of the sun's disk (if not the disk itself) will still be visible at 0.94μ even through Titan's scattering haze. Scattering effects, and possible influences of discrete clouds, mean it would take some effort to implement a robust sun position detection autonomously, but post-hoc analysis with radiative transfer models should allow the position to be measured accurately on the ground. Transformation into the Titan-centered frame of reference would require additional attitude information (possibly available from Inertial Measurement Unit IMU data, or by taking long series of position fixes such that wave motion can be averaged out). More efficient, and likely more accurate and reliable, is to adopt a sextant-like approach, and acquire an image that shows both the sun and the horizon in the same frame. This allows the sun height to be measured in the Titan frame directly to $\sim 0.2^\circ$.

Because the sun and earth are always within 6° of each other as seen from Titan, contours of equal Doppler (roughly speaking parallel to the Earth line) and contours of equal solar elevation

(roughly perpendicular to the sun line) are near-orthogonal, making for an efficient navigational solution—see Fig. 16.

The inner shaded region in Fig. 1 corresponds to a solar elevation uncertainty of 0.2° , and the outer region to 1° . Naturally, these map into widths that correspond to roughly 1° of latitude. The corresponding Doppler regions are shown—the inner Doppler region (actually smaller than the symbols denoting the locus) corresponds to a 1 mm/s measurement uncertainty. The wider region corresponds to an uncertainty of 0.1 m/s, a reasonable value for the drift rate.

6.3. VLBI

By comparing the received phase of a signal detected at two or more widely separated radio telescopes and comparing with that of known astronomical targets, the position of the source in the sky (i.e. relative to those astronomical targets) can be determined with exceptional precision. This approach has been applied to the VEGA balloons at Venus in 1984, and more recently to the Huygens probe at Titan, where position determinations of the order of 1 km precision were made.

Performing VLBI may involve a substantial analysis effort. Provision of specialized receivers was required for Huygens (although careful selection of downlink frequency may eliminate that need). The effort is simplified if small radio telescopes can be used, which will depend on the Effective Isotropic Radiated Power (EIRP) and bandwidth of the transmitted signal. Note that since the Earth is low in the sky as seen from Titan's polar regions, a ± 1 km uncertainty circle projects into a long ellipse on the surface (e.g. with the Earth 10° above the horizon, the long axis of the ellipse is ± 5 km.)

6.4. Position determination

If the vehicle were static, then a crude position determination could be accomplished over a Titan day with sun fixes alone since Titan rotates under the contours of solar elevation angle, such that contours for observations a large fraction of a Titan day apart are nonparallel—see Fig. 16. A rather more precise determination could likely be performed with Doppler-only data over the course of a Titan day—see Figs. 16 and 17.

In practice, the position and velocity of the lander would be determined on the ground as a function of time using an optimal

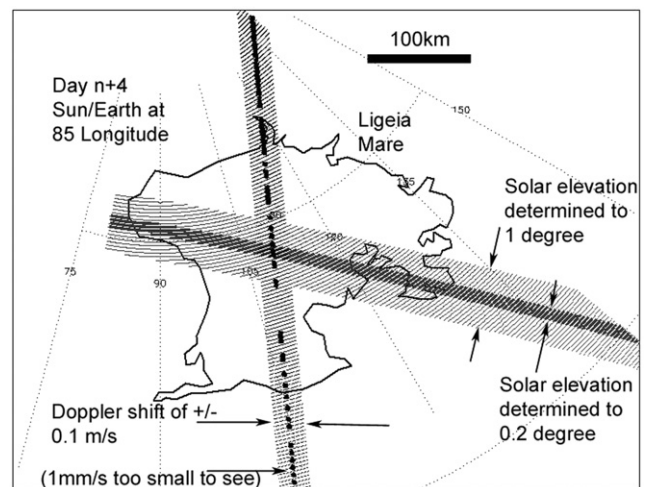


Fig. 16. Ligeia Mare with regions with a given solar elevation and earth Doppler (with specified uncertainties) indicated. The near-orthogonality of these measures means that if they can be simultaneously determined, the spacecraft lies in a usefully small intersection region.

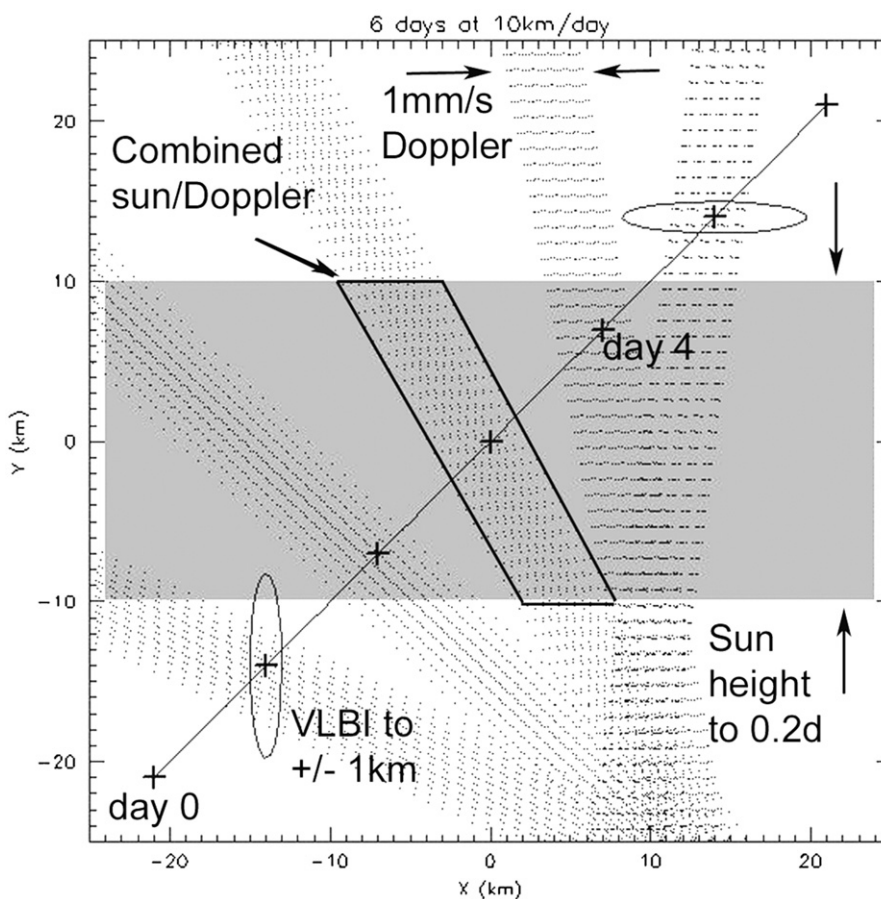


Fig. 17. Schematic of expected drift rates (starting at lower left, drifting 60 km over 6 days) and position determination accuracies. At 10 km/day (~ 10 cm/s) VLBI may be precise enough to detect a change in position over a single 8 h communications pass, and requires no a priori assumptions. With bootstrapping (i.e. assumed drift rate) Doppler navigation can be fairly precise, and in combination with sun height sensing, can give an adequate measure of position (box outline). The sun height alone is too coarse to reliably detect drift over less than ~ 4 days. Note the convergence of the Doppler solutions at ($X=10$, $Y=-25$)—since Titan's rotation sweeps the Doppler contours around in azimuth alone a reasonable position can be determined over several days by Doppler alone. The VLBI position uncertainty of a 2 km diameter circle in the plane of the sky projects into a $\sim 10 \times 2$ km ellipse near the north pole, although the long axis of the ellipse rotates once per Titan day, so two solutions 4 days apart for a fixed position would recover the full potential accuracy of VLBI.

estimator such as a Kalman filter, which weights the various observations (Doppler, sun and VLBI measurements) by their respective accuracies, together with the 'dead reckoning' estimate of the new position propagated forward from the previously computed position and velocity. We may note that this Kalman estimation approach is widely used in aerospace guidance problems, has been applied to marine tracking of tuna (e.g. Sibert et al., 2003) and was applied to the Huygens probe trajectory (Aboudan et al., 2008). Although it is likely that sun-height measurements will contribute only little to a post-hoc position history, since their accuracy is poor compared with the Doppler, they are important in generating an early position fix.

We will note in passing that as the lake edge is approached, features might be recognized in shoreline imagery which could be mapped with Cassini SAR data. Features 500 m tall will be geometrically above the horizon from distances of 50 km.

Because the interpretation of Doppler measurements into position is influenced by the instantaneous velocity, the drift trajectory reconstruction can be made more swift and accurate by a good estimate of the starting point. The foregoing discussion suggests that position recovery to 1–5 km within the first few measurements should be quite feasible, and that this precision is adequate to measure the wind drift trajectories described earlier. The accumulation of successive measurements will improve the accuracy of the back-propagated trajectory, however, a full

simulation of the position recovery process is beyond the scope of the present paper.

7. Propulsion and drag modulation

Clearly, if it were desired to move in a given direction (or equivalently stationkeep against the wind) the propulsive capability should exceed the wind drag force. Adopting a conservative drag coefficient of $C_{da}=1.0$ and using the 1 m/s wind-speeds discussed in Section 3 as a design value, the propulsive thrust required is ~ 0.5 N. Such a thrust could be generated easily by a small (< 20 cm) propeller or a pumped jet (consider that the reaction force on a typical garden hosepipe can be several times this value.)

Another possibility to consider, albeit one that offers less certainty in operation than a propeller, is some means of modulating the drag on the vehicle, for example by erecting or inflating a fabric structure to act as a sail. A mesh or similar 'tent' propped up by a mast could be reversibly raised by a single actuator and thus would be comparatively inexpensive to implement.

Drag modulation is readily simulated in the drift model above by inserting a control statement in the simulation, such that the drift is generally 0.1 times the windspeed $V=0.1U$, and $0.2U$ when

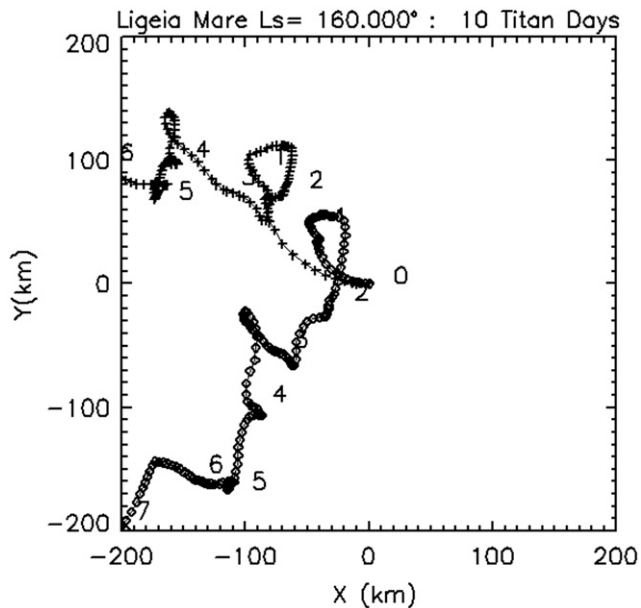


Fig. 18. Drift (as Fig. 13) but with the drift velocity doubled when the north–south wind component is in a desired direction—plus signs correspond to doubling the ratio of drift speed to windspeed when the meridional component is northwards, diamonds when it is southwards. The resultant trajectories have a substantial bias in the desired directions.

the wind (sensed, for example, by an onboard weather station) is close to the desired direction of drift. Fig. 18 shows the trajectories for the same wind history as Fig. 14, but with the logic $V=0.2U$ actuated when the meridional component is in a desired direction. It can be seen that net northwards and net southwards drift can be achieved, suggesting that even this modest control authority is able to yield a desired trajectory.

8. Conclusions

When the Huygens probe was designed, virtually nothing was known about Titan's surface or near-surface conditions. As discussed in this paper, the situation has dramatically changed for the next generation of Titan exploration vehicles—modeling tools are available to explore the possible range of day-to-day variations in meteorological properties. We have considered the conditions specifically at Ligeia Mare for late northern summer, an epoch relevant for a proposed NASA Discovery mission, TiME.

The windspeeds during the TiME season are somewhat consistent across the different models and model parameters, with typical speeds of ~ 0.5 m/s, and not exceeding 1.3 m/s. Wind directions differ significantly between models, and may be prograde or retrograde, and the north–south component is comparable with the zonal component.

Tides in Ligeia have been evaluated—the principal effect is a slosh between the eastern and western lobes, where an amplitude of ~ 0.6 m is encountered. Tidal currents depend on depth, and for a likely central depth of several hundred meters are ~ 1 cm/s: a clockwise flow pattern forms in the center of Ligeia. These tidal currents are enough to cause significant mixing and suspension of mm-size solids even in seasons without convective mixing. However, the motion of a capsule is likely dominated by wind drag.

We find that a capsule is likely to drift at about one tenth of the windspeed, unless design measures are taken to augment the above- or below-waterline drag areas. In this case, a drift of some

10 s of km per day is possible, and will be readily measurable by a variety (and in particular, by a combination) of techniques. Since the wind vector rotates in azimuth throughout a Titan day, drag modulation with a single actuator can be an effective means of controlling the drift.

Acknowledgements

TT acknowledges support from the DFG. CN is supported by the OPR and NAI, also using resources provided by the NASA High-End Computing (HEC) Program through the NASA Advanced Supercomputing (NAS) Division at Ames Research Center. We acknowledge Ellen Stofan, Jonathan Lunine and the Lockheed, APL and Science teams of TiME for stimulating this work. Fig. 1 is derived from a mosaic originally by Alex Hayes. We acknowledge the comments of Jason Barnes and an anonymous reviewer for comments that improved the manuscript.

References

- Achterberg, R.K., Conrath, B.J., Gierasch, P.J., Flasar, F.M., Nixon, C.A., 2008. Titan's middle-atmospheric temperatures and dynamics observed by the Cassini composite infrared spectrometer. *Icarus* 194, 263–277.
- Aboudan, A., Colombatti, G., Ferri, F., Angrilli, F., 2008. Huygens probe entry trajectory and attitude estimated simultaneously with Titan atmospheric structure by Kalman filtering. *Planetary and Space Sciences* 56, 573–585.
- Aharonson, O., Hayes, A., Lunine, J.I., Lorenz, R.D., Elachi, C., 2009. An asymmetric distribution of lakes on Titan as a possible consequence of orbital forcing. *Nature Geoscience* 2, 851–854.
- Barnes, J., Soderblom, J.M., Brown, R.H., Soderblom, L.A., Stefan, K., Jaumann, R., Le Mouelic, S., Rodriguez, S., Sotin, C., Buratti, B.J., Baines, K.H., Clark, R.N., Nicholson, P.D., 2011. Wave constraints for Titan's Jingpo Lacus and Kraken Mare from VIMS specular reflection lightcurves. *Icarus* 211, 722–731.
- Brown, R.H., Soderblom, L.A., Soderblom, J.M., Clark, R.N., Jaumann, R., Barnes, J.W., Sotin, C., Buratti, B., Baines, K.H., Nicholson, P.D., 2008. The identification of liquid ethane in Titan's Ontario Lacus. *Nature* 454, 607–610. doi:10.1038/nature07100.
- Cordier, D., Mousis, O., Lunine, J.I., Lavvas, P., Vuitton, V., 2009. An estimate of the chemical composition of Titan's lakes. *Astrophysical Journal* 707, L128–L131.
- Dermott, S.F., Sagan, C., 1995. Tidal effects of disconnected hydrocarbon seas on Titan. *Nature* 374, 238–240.
- Ebbemeyer, C., 2009. Flotsametrics and the Floating World: How One Man's Obsession with Runaway Sneakers and Rubber Ducks Revolutionized Ocean Science. Smithsonian Publishers.
- Hayes, A.G., Wolf, A.S., Aharonson, O., Zebker, H., Lorenz, R., Kirk, R.L., Paillou, P., Lunine, J., Wye, L., Callahan, P., Wall, S., Elachi, C., 2010. Bathymetry and absorptivity of Titan's Ontario Lacus. *Journal of Geophysical Research: Planets* 115, E09009.
- Hill, R., 1994. Theory of geolocation by light levels. In: Physiology, B.J., LeBoeuf, L., Laws, R.M. (Eds.), *Elephant Seals: Population Ecology, Behaviour, and*. University of California Press, Berkeley, CA, pp. 227–236.
- Janssen, M.A., Lorenz, R.D., West, R., Paganelli, F., Stiles, B., Wall, S.D., Callahan, P., Kirk, R.L., Roth, L., Anderson, Y., 2009. The Cassini Radar Team, Titan's surface at 2.2-cm wavelength imaged by the Cassini RADAR radiometer: Calibration and first results. *Icarus* 200, 222–239.
- Jennings, D.E., Flasar, F.M., Kunde, V.G., Samuelson, R.E., Pearl, J.C., Nixon, C.A., Carlson, R.C., Mamoutkine, A.A., Brasunas, J.C., Guandique, E., Achterberg, R.K., Bjoraker, G.L., Romani, P.N., Segura, M.E., Albright, S.A., Elliott, M.H., Tingley, J.S., Calcutt, S., Coustenis, A., Courtin, R., 2009. Titan's surface brightness temperatures. *Astrophysical Journal Letters* 691, L103–L105.
- Kirwan, A.D., McNally, G., Chang, M.S., Molinari, R., 1975. The effect of wind and surface currents on drifters. *Journal of Physical Oceanography* 5, 361–368.
- Lorenz, R.D. Huygens Probe—The Surface Mission, In: Kaldeich, B. (Ed.), *Proceedings of the Symposium on Titan, Toulouse, September 1991*. ESA SP-338, European Space Agency, Noordwijk, pp. 359–364 1992.
- Lorenz, R.D., 1994. Crater lakes on Titan: Rings, horseshoes and bullseyes. *Planetary and Space Science* 42, 1–4.
- Lorenz, R.D., 1996. Martian surface windspeeds, described by the Weibull distribution. *Journal of Spacecraft and Rockets* 33, 754–756.
- Lorenz, R.D., Kraal, E., Asphaug, E., Thomson, R., 2003. The Seas of Titan. *EOS* 84, 125–132.
- Lorenz, R.D., Kraal, E., Eddlemon, E., Cheney, J., Greeley, R., 2005. Sea-surface wave growth under extraterrestrial atmospheres—Preliminary wind tunnel experiments with application to Mars and Titan. *Icarus* 175, 556–560. Lorenz, R.D., Mitchell, K.L., Kirk, R.L., Hayes, A.G., Zebker, H.A., Paillou, P., Radebaugh, J., Lunine, J.I., Janssen, M.-A., Wall, S.D., Lopes, R.M., Stiles, B., Ostro, S., Mitri, G., Stofan, E.R., 2008. and the Cassini RADAR Team. Titan's Inventory of Organic Surface Materials. *Geophysical Research Letters* 35, L02206.

- Lorenz, R.D., Newman, C., Lunine, J.I., 2010. Threshold of wave generation on Titan's lakes and seas: Effect of viscosity and implications for Cassini observations. *Icarus* 207, 932–937.
- Lunine, J.I., Plausible surface models for Titan. In: Kaldeich, B. (Ed.), Proceedings of the Symposium on Titan, Toulouse, September 1991. ESA SP-338, European Space Agency, Noordwijk, pp. 233–239, 1992.
- Mitri, G., Showman, A.P., Lunine, J.I., Lorenz, R.D., 2007. Hydrocarbon lakes on Titan. *Icarus* 186, 385–394.
- Newman, C., M.I. Richardson, C. Lee, A.D. Toigo, S.P. Ewald, The TitanWRF Model at the end of the Cassini Prime Mission, American Geophysical Union, Fall Meeting 2008, abstract #P12A-02, 2008.
- Newman, C., C. Lee, Y. Lian, M.I. Richardson, A.D. Toigo, Stratospheric superrotation in the TitanWRF Model, submitted to *Icarus*, November 2010.
- Paillou, P., Mitchell, K., Wall, S., Ruffie, G., Wood, C., Lorenz, R., Stofan, E., Lunine, J., Lopes, R., Encrenaz, P., 2008. Microwave dielectric constant of liquid hydrocarbons: Application to the depth estimation of Titan's lakes. *Geophysical Research Letters* 35, L05202.
- Richardson, M.I., Toigo, A.D., Newman, C.E., 2007. PlanetWRF: A general purpose, local to global numerical model for planetary atmospheric and climate dynamics. *Journal of Geophysical Research* 112, E09001.
- Sagan, C., Dermott, S.F., 1982. The tide in the seas of Titan. *Nature* 300, 731–733.
- Sears, W.D., 1995. Tidal dissipation in oceans on Titan. *Icarus* 113, 39–56.
- Sibert, J., Musyl, M.K., Brill, R.W., 2003. Horizontal movements of bigeye tuna (*Thunnus obesus*) near Hawaii determined by Kalman filter analysis of archival tagging data. *Fisheries and Oceanography* 12, 141–151.
- Sohl, F., Sears, W.D., Lorenz, R.D., 1995. Tidal dissipation on Titan. *Icarus* 115, 278–294.
- Stephan, K., Jaumann, R., Brown, R.H., Soderblom, J.M., Soderblom, L.A., Barnes, J.W., Sotin, C., Griffith, C.A., Kirk, R.L., Baines, K.H., Buratti, B.J., Clark, R.N., Lytle, D.M., Nelson, R.M., Nicholson, P.D., 2010. Specular reflection on Titan: Liquids in Kraken Mare. *Geophysical Research Letters* 37, L07104.
- Stofan, E.R., Elachi, C., Lunine, J.I., Lorenz, R.D., Stiles, B., Mitchell, K., Ostro, S., Soderblom, L., Wood, C., Zebker, H., Wall, S., Janssen, M., Kirk, R., Lopes, R., Paganelli, F., Radebaugh, J., Wye, L., Anderson, Y., Allison, M., Boehmer, R., Callahan, P., Encrenaz, P., Flamini, E., Francescetti, G., Gim, Y., Hamilton, G., Hensley, S., Johnson, W.T.K., Kelleher, K., Muhleman, D., Paillou, P., Picardi, G., Posa, F., Roth, L., Seu, R., Shaffer, S., Vetrella, S., West, R., 2007. The Lakes of Titan. *Nature* 441, 61–64.
- Stofan, E.R., J.I. Lunine, R.D. Lorenz, O. Aharonson, E. Bierhaus, B. Clark, C. Griffith, A.-M. Harri, E. Karkoschka, R. Kirk, B. Kantsiper, P. Mahaffy, C. Newman, M. Ravine, M. Trainer, H. Waite, J. Zarnecki. Exploring the Seas of Titan: The Titan Mare Explorer (TiME) Mission, 41st Lunar and Planetary Science Conference, Abstract #1236, Lunar and Planetary Institute, Houston, TX, March 2010.
- Tokano, T., 2009a. Impact of seas/lakes on polar meteorology of Titan: Simulation by a coupled GCM-Sea model. *Icarus* 204, 619–636.
- Tokano, T., 2009b. Limnological structure of Titan's hydrocarbon lakes and its astrobiological implication. *Astrobiology* 9, 147–164.
- Tokano, T., 2010. Simulation of tides in hydrocarbon lakes on Saturn's moon Titan. *Ocean Dynamics* 60, 803–817.
- Turtle, E., Perry, J.E., McEwen, A.S., DeGenio, A.D., Barbara, J., West, R.A., Dawson, D.D., Porco, C., 2009. Cassini imaging of Titan's high-latitude lakes, clouds, and south-polar surface changes. *Geophysical Research Letters* 36, L02204.